Dynamics and Function in a Bacterial ABC Transporter: Simulation Studies of the BtuCDF System and Its Components†

Anthony Ivetac, Jeff D. Campbell, and Mark S. P. Sansom*

Department of Biochemistry, University of Oxford, South Parks Road, Oxford, OX1 3QU, U.K.

Received November 1, 2006; Revised Manuscript Received December 21, 2006

ABSTRACT: ABC transporters are integral membrane proteins which couple the energy of ATP hydrolysis to the translocation of solutes across cell membranes. BtuCD is a ∼1100-residue protein found in the inner membrane of Gram-negative bacteria which transports vitamin B_{12}. Vitamin B_{12} is bound in the periplasm by BtuF, which delivers the solute to the periplasmic entrance of the transporter protein complex BtuCD. Molecular dynamics simulations of the BtuCD and BtuCDF complexes (in a lipid bilayer) and of the isolated BtuD and BtuF proteins (in water) have been used to explore the conformational dynamics of this complex transport system. Overall, seven simulations have been performed, with and without bound ATP, corresponding to a total simulation time of 0.1 μs. Binding of ATP drives closure of the nucleotide-binding domains (NBDs) in BtuD in a symmetrical fashion, but not in BtuCD. It seems that ATP constrains the flexibility of the NBDs in BtuCD such that their closure may only occur upon binding of BtuF to the complex. Upon introduction of BtuF, and concomitant with NBD association, one ATP-binding site displays a closure, while the opposite site remains relatively unchanged. This asymmetry may reflect an initial step in the "alternating hydrolysis" mechanism and is consistent with measurements of nucleotide-binding stoichiometries. Principal components analysis of the simulation of BtuCD reveals motions that are comparable to those suggested in current transport models.

The ATP-binding cassette (ABC[1]) transporters form a superfamily of integral membrane proteins, in both prokaryotes and eukaryotes, which couple the energy of ATP hydrolysis to the translocation of solutes across cell membranes. The transported species (solutes, also known as allocrites) include polypeptides (e.g., TAP (*1*)), ions (e.g., CFTR (*2*)), sugars (e.g., $MalFGK_2$ (*3*)), lipids (e.g., MsbA (*4*)), other hydrophobic compounds (e.g., P-glycoprotein (*5*)), and amino acids (e.g., $HisQMP_2$ (*6*)). ABC transporters are generally classed as either exporters or importers, depending on the direction of transport of the solute. The majority of prokaryotic ABC transporters act as importers, while all known eukaryotic ABC transporters are exporters (*7*). ABC transporters are of biomedical relevance in the context of, e.g., antibiotic resistance (*8*), poor responses to chemotherapy (*9*), and cystic fibrosis (*10*).

The archetypal ABC transporter is composed of four core domains: two transmembrane domains (TMDs), and two nucleotide-binding domains (NBDs). These can be arranged in a variety of topologies (*11*). The TMDs reside in the membrane and consist of multiple transmembrane α-helices which span the lipid bilayer and form the binding site and translocation pathway for the solute. The TMDs of ABC transporters show rather low sequence similarity when compared to one another, which may be linked to the wide range of transported species. It is thought that the TMDs may possess one or more pairs of high- and low-affinity solute binding sites, with the solute binding to the high-affinity site and then being passed to the low-affinity site and onto its interior or exterior destination (*12*). The TMDs of bacterial ABC importers typically interact with a periplasmic binding protein (PBP), which sequesters the solute in the periplasm and delivers it to the TMDs, thus helping to confer specificity. The NBDs are intracellular, water-soluble domains/subunits which drive the transport cycle by binding and hydrolysis of ATP. ATP hydrolysis is thought to drive a conformational change in the NBDs which propagates to the TMDs, leading to translocation of the solute. Unlike the TMDs, the NBDs are highly conserved, suggestive of their universal role in powering the transport process. They are composed of an ABC domain, which contains a Walker A and Walker B motif (common to many ATP-binding domains), the Signature sequence (C motif), which defines the ABC transporter, and several other functionally important sites. The Walker A and B motifs, housed on the F1-like ATP-binding core, are thought to have a role in binding the phosphates of ATP and the Mg^{2+} ion which is bound to the ATP, respectively, while the Signature sequence, housed on an α-helical subdomain, is proposed to complete the ATP-binding site initiated by the Walker A and B motifs of the other NBD (*13*).

† Research in M.S.P.S.'s laboratory is supported by the BBSRC and the Wellcome Trust. A.I. was supported by MRC, and J.D.C. by the Wellcome Trust.

* To whom correspondence should be addressed. E-mail: mark.sansom@bioch.ox.ac.uk. Phone: +44-1865-275371. Fax: +44-1865-275273.

[1] Abbreviations: ABC, ATP-binding cassette; DMPC, dimyristoyl phosphatidylcholine; PC, phosphatidylcholine; PCA, principal components analysis; PME, particle mesh Ewald; NBD, nucleotide binding domain; RMSD, root mean square deviation; TMD, transmembrane domain.

10.1021/bi0622571 CCC: $37.00
Published on Web 02/16/2007

Table 1: Summary of Simulations

simulation	components	number of atoms	duration restrained (ns)	duration unrestrained (ns)
BtuD	NBDs	~70 000	0.2	15
BtuD−ATP	NBDs + ATP	~70 000	0.2	15
BtuCD	NBDs + TMDs	~115 000	0.2	15
BtuCD−ATP	NBDs + TMDs + ATP	~115 000	0.2	15
BtuF	PBP	~40 000	0.2	20
BtuCDF	NBDs + TMDs + PBP	~140 000	0.2	10
BtuCDF−ATP	NBDs + TMDs + PBP +ATP	~140 000	0.2	10

The majority of the high-resolution structural data available for ABC transporters are for the NBDs, reflecting their solubility and hence relative ease of expression and crystallization. In contrast, high-resolution structures are known for only three complete ABC transporters: MsbA (*14*−*16*), BtuCD (*17*), and the SAV1866 multidrug transporter (*18*).

BtuCD is a 1110-residue protein found in the inner membrane of various Gram-negative bacteria. It plays a central role in vitamin B_{12} uptake. Vitamin B_{12} is sequestered in the periplasm by the PBP (BtuF), which delivers the solute to the periplasmic entrance of BtuCD (*19*). BtuCD consists of two copies each of the BtuC (TMD) and BtuD (NBD) subunits. Each TMD is composed of ten transmembrane α-helices, and there is a cavity present at the periplasmic end of the inter-TMD space which is large enough to accommodate much of a vitamin B_{12} molecule, although there is no solute bound in the X-ray structure. Two serine-threonine pairs block the cytoplasmic entrance to the translocation pathway to form a putative "gate" region. Two short helices at each TMD−NBD interface ("L-loops") are proposed to play a role in the transfer of conformational change from the NBDs to the TMDs. The NBDs follow the canonical ABC domain fold of other ABC transporters, and the dimer is arranged in a similar fashion to Rad50cd (*20*), with the nucleotide-binding sites sandwiched between the Walker A motif of one NBD and the Signature sequence of the opposite NBD. A vanadate species (cyclotetrametavanadate) was present at the nucleotide-binding site, with two of the vanadate atoms superimposing well with the α and γ phosphates of docked ADP/ATP.

The nature of the conformational changes in ABC transporters in relationship to the mechanism of transport remains elusive (*21*), although some progress has been made via comparison with multiple structures for MsbA (*22*). One approach which may be adopted to explore the conformational dynamics of membrane proteins is that of molecular dynamics (MD) simulations (*23*, *24*). MD simulations have been employed as a computational tool to study the conformational dynamics of a wide range of membrane proteins (*25*, *26*). They have been applied to ABC transporter NBDs, such as the MJ0796 NBDs (*27*) and the HisP NBDs (*28*, *29*), as well as a low-resolution structure of the complete MsbA molecule (*30*). More recently, the BtuCD protein was simulated using explicit (*31*) and implicit (*32*) bilayer MD techniques. These simulations suggest that, in the full transporter, ATP binding leads to NBD closure, with the ATP-binding sites acting in an asymmetrical fashion. However, a more comprehensive simulation study of the relationship between the conformational dynamics of BtuCD and the presence/absence of bound ATP, and the influence of interactions with the periplasmic binding protein BtuF is required.

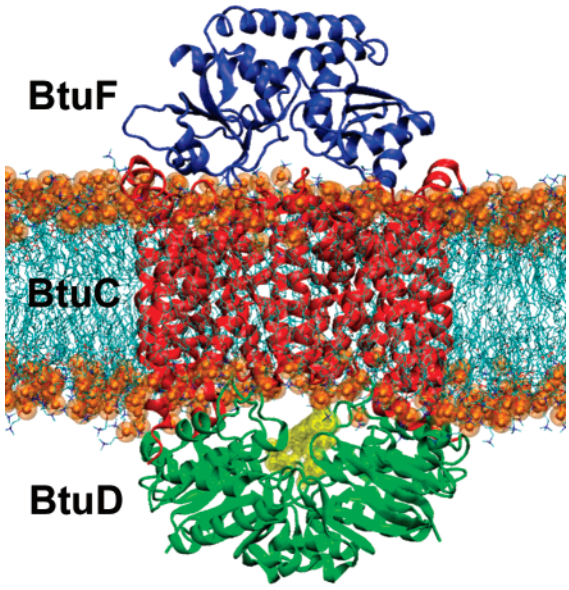

FIGURE 1: Simulation components. Protein subunits shown in cartoon representation. BtuF is colored blue, BtuC is colored red, and BtuD is colored green. Bound ATP molecules are colored yellow. The BtuCDF complex is embedded in a DMPC bilayer, with headgroup phosphorus atoms in orange and the hydrophobic tails of the lipids in blue.

In the current study, we use multiple MD simulations to explore the dynamic behavior of the various components of the BtuCDF import complex, in different configurations. In particular, we aim to understand the changes which take place upon nucleotide-binding, the principal motions of the transporter, and the role of the PBP, which may help understand the mechanism of transport.

EXPERIMENTAL PROCEDURES

Simulation System Design. Two initial systems (See Table 1 and Figure 1) were set up to explore the conformational dynamics of BtuCD: (i) an approximation of the physiological environment, whereby the entire protein (i.e., $BtuC_2D_2$) is inserted into a solvated lipid (dimyristoyl phosphatidylcholine, DMPC) bilayer; and (ii) an isolated NBD dimer (i.e., $BtuD_2$) in a box of water. The latter system was explored given the observation (see, e.g., (*33*)) that NBD dimers with ATPase activity can form independently of the TMDs. The $BtuD_2$ simulation also permits exploration of the dynamics of the NBDs without the constraint of the neighboring bilayer-embedded TMDs. For each system, two simulations were run (see Table 1): (i) in the absence of any ligand at the nucleotide-binding site; and (ii) with Mg^{2+}-ATP bound at each site. These enabled us to explore the effect of presence/absence of a nucleotide ligand on the protein.

Two further systems were set up to explore the role and influence of the PBP on the transporter. First, the water-soluble BtuF subunit was simulated on its own in water (noting that a simulation study of BtuF has been published recently (*34*)). This structure was also docked onto BtuCD to form a complete transport complex (BtuCDF), and again simulated with and without Mg^{2+}-ATP bound at each site.

System Preparation and Simulations. Coordinates for BtuCD and BtuF were used as downloaded from the RSCB (http://www.rcsb.org, entries 1L7V (*17*) and 1N4D, respectively (*19*)). The only modification from the downloaded coordinates was the removal of the two bound cyclotetrametavanadate molecules from the BtuCD structure.

A pre-equilibrated DMPC bilayer of 576 molecules formed the basis of subsequent membrane-inserted simulations. The TMDs were inserted in this bilayer and oriented using bands of charged residues to determine the optimal position of the protein relative to the bilayer. DMPC molecules overlapping the protein were removed, and the resultant TMD/bilayer system was solvated, energy-minimized, and equilibrated for 1 ns, with the non-H atoms of the TMDs restrained (force constant = 1000 kJ mol^{-1} nm^{-2}) in order to allow a relaxation of the packing of lipids around the protein. The NBDs were then docked back (by least-squares superposition) onto the TMDs, and the complete system was further equilibrated with all protein non-H atoms restrained for 0.2 ns. For the NBD dimer simulations, the NBDs were solvated, energy-minimized, and equilibrated with protein non-H atoms restrained for 0.2 ns. This procedure was repeated for the simulation of BtuF alone.

In order to generate the BtuCDF complex, it was necessary to dock the BtuF subunit onto BtuCD. BtuF was manually docked onto BtuCD, using the approach adopted by Borths et al. (*35*) whereby the conserved glutamates (residues 72 and 202) on each lobe of BtuF was placed in close proximity to conserved patches of arginines (residues 56, 59, and 295) on the periplasmic surface of BtuC. This enables a favorable electrostatic interaction between each lobe of BtuF and its corresponding TMD, and aligns the vitamin B_{12}-binding site over the putative translocation pathway. Subsequently, HeX (http://www.csd.abdn.ac.uk/hex) was used to generate an ensemble of complexes around this manual docking from which the lowest interaction energy configuration was selected. The final BtuCDF complex was generated by using structures of BtuCD and BtuF taken from the equilibrated portions of their respective simulations, as this yielded a better docking score than did the crystal structures (structures at 5 ns were taken in all cases).

Mg^{2+}-ATP was docked into the NBDs using the MJ0796 NBD dimer structure (PDB code 1L2T) as a template. The Na-ATP coordinates from MJ0796 were superimposed onto each BtuD subunit by least-squares fitting of residues from the Walker A and Walker B motifs and the Q-loop. It was then assumed that the Mg^{2+} ion binds to the same coordinates as the Na^{+} ion. For the BtuCDF-ATP simulation, ATP coordinates were taken from the 5 ns snapshot of the BtuCD-ATP simulation.

All energy minimization was performed using 100 steps of the steepest descents algorithm. Equilibration was performed using harmonic restraints on the protein non-H atoms (and ATP when present) (force constant = 1000 kJ mol^{-1} nm^{-2}), a Berendsen thermostat (*36*), and pressure maintained at 1 bar by a Berendsen barostat (*36*). The unrestrained production runs were performed with a Nosé−Hoover thermostat (*37*, *38*) and pressure maintained at 1 bar by a Parrinello−Rahman barostat (*39*). The simulations were run in the NPT ensemble and at a temperature of 310 K. Particle mesh Ewald (PME) was used to treat long-range electrostatics (*40*), and the single point charge (SPC) water model (*41*) was used for the solvent. Chloride anions were positioned randomly among the solvent to neutralize the system. The integration time step was 2 fs, and coordinates were saved every 5 ps for subsequent analysis. The LINCS algorithm was used to restrain all bond lengths (*42*).

Simulations were run and analyzed using the *GROMACS* v. 3.1 (http://www.gromacs.org) molecular dynamics simulation package (*43*−*45*) with the GROMOS96 forcefield (*46*). Lipid parameters were based on those described in (*47*). Pore profiles were calculated using HOLE (*48*). 3D graphics were produced using VMD (*49*) and Pymol (http://www.pymol.org).

RESULTS

Conformational Drift. To assess the degree of conformational drift of the protein during the BtuD and BtuCD simulations, the root mean square deviation (RMSD) of Cα atoms, with respect to the starting conformation, was calculated as a function of time (summarized in Table 2). The all-residue Cα RMSD of each simulation is characterized by a steep initial rise in RMSD for approximately 0.5 ns (data not shown), as is characteristic of membrane protein simulations. The two BtuCD systems subsequently plateau at a RMSD of 0.25 to 0.3 nm for the remainder of the simulation. In contrast, the BtuD simulations exhibit more substantial fluctuations in their all residue Cα RMSDs, and indeed do not seem to have converged within 15 ns (see Figure 2). The contrast in degree of conformational drift in the two environments probably reflects the relative freedom of the NBDs in the BtuD dimer in water, compared to when they are components of the intact transporter, which is restricted by the surrounding DMPC bilayer and by more substantial protein−protein contacts.

One may also compare Cα RMSDs (Table 2) to analyze patterns of conformational drift within, and between, domains/subunits (see, e.g., (*50*) for a discussion of such analysis to examine interdomain motions in a receptor protein). If one compares the RMSD of the TMD dimer to the individual RMSDs of each TMD (see Table 2), it is evident that much of the drift is accounted for by interdomain motion, i.e., of the two TMDs relative to one another. Examining the RMSDs of the BtuCD simulations reveals that, after the initial rise, the TMDs in the two simulations both settle to a reasonably stable conformation for the remainder of the simulation (data not shown). The TMDs of BtuCD-ATP stabilize at an average Cα RMSD relative to the starting structure of ∼0.18 nm, while those of BtuCD (i.e., in the absence of nucleotide) drift to ∼0.2 nm.

Turning to the RMSDs of both NBDs for each simulation (see Table 2), we see a more substantial degree of conformational drift. This is true for all NBDs except those in simulation BtuCD-ATP, for which the RMSD plateaus at ∼0.22 nm after around 5 ns. For all other NBD dimers, the structure drifts for the entire simulation. If one examines the

Table 2: Conformational Drift[a]

simulation name	components	RMSD (nm)
BtuD	all residues	0.30
	NBD1	0.26
	NBD2	0.23
BtuD−ATP	all residues	0.28
	NBD1	0.18
	NBD2	0.25
BtuCD	all residues	0.29
	TMDs	0.22
	NBDs	0.29
	TMD1	0.21
	TMD2	0.19
	NBD1	0.20
	NBD2	0.18
BtuCD−ATP	all residues	0.28
	TMDs	0.21
	NBDs	0.22
	TMD1	0.18
	TMD2	0.17
	NBD1	0.15
	NBD2	0.16
BtuF	all residues	0.28
BtuCDF*	all residues	0.29
	TMDs	0.26
	NBDs	0.26
	TMD1	0.23
	TMD2	0.22
	NBD1	0.23
	NBD2	0.25
	BtuF	0.25
BtuCDF−ATP*	all residues	0.36
	TMDs	0.26
	NBDs	0.24
	TMD1	0.24
	TMD2	0.23
	NBD1	0.21
	NBD2	0.21
	BtuF	0.27

[a] Average root mean square deviation (RMSD) of Cα atoms were calculated, relative to the starting structure, for the final 10 ns (or *5 ns) of each simulation.

RMSDs of the individual NBDs of BtuCD (Figure 2), it can be seen that all NBDs maintain a stable RMSD after 1−2 ns. Interestingly, the degree of drift shows a dependence on the presence/absence of bound nucleotide and is ∼0.07 nm lower for the NBDs in the BtuCD-ATP simulation than in the BtuCD simulation (see Table 2). This suggests that the nucleotide may constrain the conformational freedom of the NBDs, through protein−nucleotide noncovalent interactions. A similar effect of bound nucleotide is seen in simulations of the isolated dimer of MJ0796 (*27*). In contrast, the RMSDs of the individual NBDs of the two BtuD simulations (Figure 2) fluctuate to a much greater extent and do not reach a plateau within 15 ns. However, on average, the degree of conformational drift of the NBDs of BtuD is lower when ATP is bound. The average RMSD across all individual NBDs of the two BtuD simulations shows a drift of 0.23 nm from the crystal structure, whereas all NBDs of the two BtuCD simulations drifted to an average of 0.17 nm. Therefore, it appears both bound nucleotide and protein−protein interactions with the TMDs can modulate the conformational dynamics of the NBDs.

Principal Components Analysis: BtuCD Simulations. Principal component analysis enables isolation of the *essential subspace* (i.e., global, concerted motions) from the local fluctuations via calculation of a set of eigenvectors which describe correlated motions of atoms within the MD simulation (*51*). These eigenvectors are sorted according to their magnitude of displacement (i.e., the eigenvalue). Thus, the largest eigenvalues describe the dominant motions within a simulation. It is possible to visualize the motion described by an eigenvector by calculating the two extreme projections on the time-averaged structure from the simulation and performing an interpolation between these extremes. This was carried out for the first five eigenvectors of each of the BtuD and BtuCD simulations. The first five eigenvectors correspond to ∼53% of the motion observed in the BtuCD simulations and ∼65% of the motion observed in the BtuD simulations. While recognizing that a 10−15 ns time scale falls far short of that required to observe a complete transport event (i.e., ≥100 ms (*52*)), it is likely that PCA can reveal aspects of the intrinsic flexibility of the TMDs which allow transport to occur. Indeed, similar analysis of, e.g., potassium channel simulations has revealed aspects of conformational changes related to channel gating (*53*, *54*).

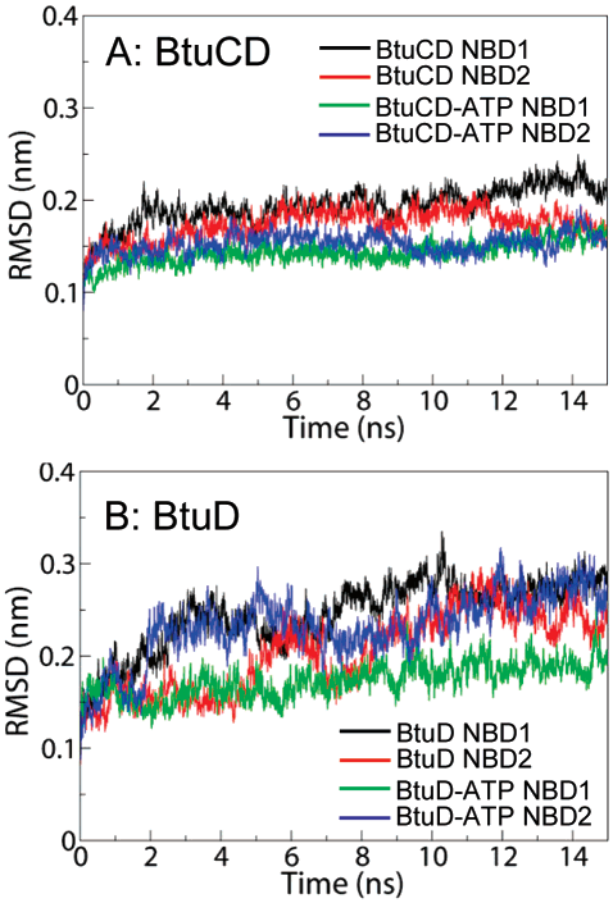

FIGURE 2: Conformational drift. A. Root mean square deviation (RMSD) of Cα atoms from the starting structure as a function of time for the NBD subunits in the BtuCD simulations. B. RMSDs for the NBDs in the BtuD simulations.

In Figure 3, we illustrate the motion described by eigenvector 1 of the BtuCD simulation in the absence of bound nucleotide. The motion corresponds to a closure of the NBDs at one ATP binding site in a rigid, concerted movement of the residues surrounding this site. The periplasmic ends of the TMDs move in opposite directions to each other, such that the TMDs "shear" against each other,

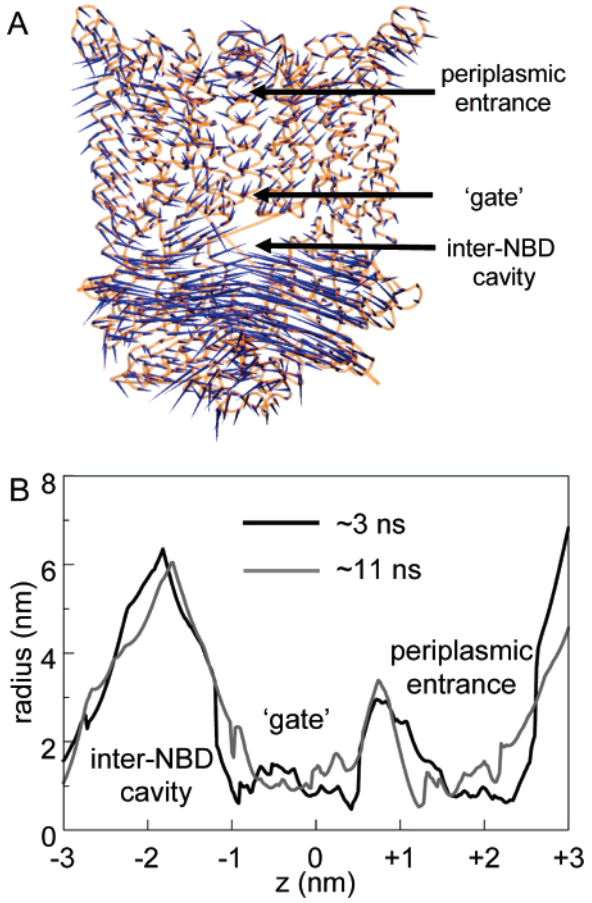

FIGURE 3: Principal components analysis of the BtuCD simulation. A. Porcupine plot of eigenvector 1 (cones denote the direction of movement of each α-carbon, from the base to the tip, with the length of the cone describing the amplitude of the motion). B. Pore radius profiles of two trajectory snapshots (at times 3 and 11 ns) which illustrate the extremes of the motion observed during the simulation.

in a symmetrical fashion. This motion is of interest, as it influences the dimensions of the porelike (presumed) translocation pathway, by prying apart the periplasmic ends of the TMDs. To investigate this further, the simulation frames with the lowest RMSDs compared to the two extreme projections of this motion were selected, and the corresponding pore radius profiles analyzed with HOLE (*48*). From the results of this analysis (Figure 3), it can be seen that the simulated closure of the NBDs coincides with a constriction at the "gate" region and an opening of the periplasmic entrance.

This motion is reminiscent of the transport model proposed by Davidson and Chen for the maltose importer $MalFGK_2$, whereby a coming together of the cytoplasmic ends and an opening of the periplasmic ends of the TMDs opens the periplasmic entrance upon NBD association (*21*). This motion also correlates with the observation (using site-directed spin labeling) that occlusion of the cytoplasmic chamber of the MsbA TMDs (in the presence of an ATP analogue) coincides with an opening of the periplasmic end of the TMDs (*55*). The inverse motion is then supposed to transfer the solute from the periplasmic entrance of the TMDs to the water-filled cavity in between all four subunits, and from there onto the cytoplasm.

It is of interest that the NBD closing motion is focused on just one of the ATP-binding sites of this homodimeric

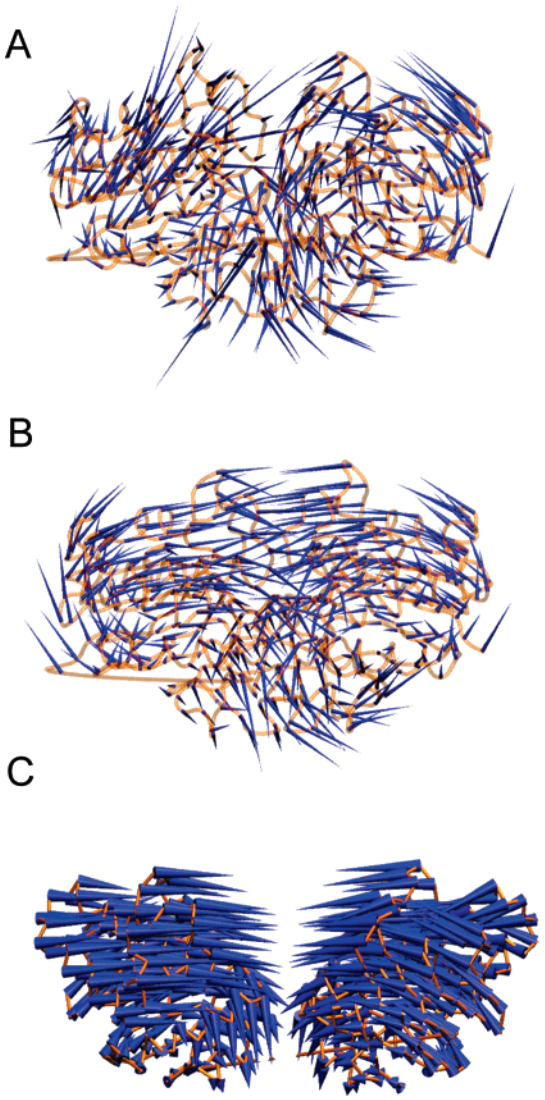

FIGURE 4: Principal components analysis of the BtuD simulations. A. Porcupine plot of the BtuD simulation (eigenvector 1). B. Porcupine plot of the BtuD ATP simulation (eigenvector 1). C. Porcupine plot of vectors derived by interpolation between the three MalK crystal structures.

structure. The alternating catalytic sites models for P-glycoprotein (a single polypeptide chain) (*56*) and for the bacterial LmrA (a homodimer) (*8*) both propose that ATP hydrolysis occurs sequentially and therefore alternates between the two NBDs. The closure at one site seen here shows that the two sites may simultaneously occupy different states, as required by an alternating cycle, and that closure at a single site can still modify the translocation pathway and TMDs. Such a motion of the NBDs is not seen in the BtuCD-ATP simulation.

Principal Components Analysis: BtuD Simulations. The motion corresponding to the principal component (eigenvector 1) of the BtuD simulations, which exhibits a relatively high displacement of Cα atoms, can be seen to be symmetrical about the inter-NBD plane (Figure 4). In both the BtuD and BtuD-ATP simulations, this motion brings the NBDs into closer association, with a resulting increase in the surface area buried between the subunits. This suggests that there is a potential opening/closing motion between the NBDs. It has been proposed that the association and dissociation of the NBDs is a crucial event in the reaction

cycle of ABC transporters, with ATP binding causing association and ATP hydrolysis causing dissociation of the NBDs. This movement is central to the ATP-switch model (*57*) and is captured by the "tweezers-like" motion seen in the MalK crystal structures (*58*), as well as the "nucleotide sandwich" arrangement which is thought to be a common feature of ABC NBDs (*59*). It is noteworthy that the NBD motion seen here is characterized by a rigid-body motion of the entire NBD, as opposed to the intra-NBD rotation of the helical domain, for example, as seen in ref 28. That such a motion is observed in our simulations even in the *absence* of nucleotide suggests that the capacity to open and close is an intrinsic property of the protein, with ATP and the products of hydrolysis driving the motion in opposing directions. It is interesting to compare this opening/closing principal component of the ATP-bound BtuD dimer to the three crystal structures of the NBDs of the maltose importer (MalK; see Figure 4). The closing motion of BtuD (particularly with ATP bound) follows a very similar path to the "transition" from the open ATP-free MalK structure to the closed ATP-bound structure.

How does the closing motion of the NBDs correlate with simulation time, with and without nucleotide? Given current biochemical evidence and transport models, e.g., (*20*, *60*, *61*), one might expect the ATP-bound BtuD dimer to associate more tightly over time and while expecting the nucleotide-free BtuD dimer to randomly undergo smaller opening and closing motions, especially in the context of the greater flexibility seen both in our simulation studies and in the multiple conformational states of the nucleotide-free GlcV NBD structures (*62*). To answer this, the BtuD and BtuD-ATP trajectories were concatenated together, and PCA was performed on this larger trajectory, according to the "combined analysis" method (*63*). The eigenvectors from this PCA would now describe motions common to both the BtuD and BtuD-ATP trajectories. The closing motion (eigenvector 1) was selected, and the individual trajectories were projected onto this eigenvector, to reveal the differences in fluctuation along this mode. The ATP-bound BtuD dimer clearly moves from one extreme to another (from an "open" to a "closed" conformation over 15 ns), while the nucleotide-free BtuD dimer fluctuates between opening and closing motions throughout the simulation. This suggests that ATP drives the NBD toward a more closed conformation, while the ATP-free dimer fluctuates between more open and more closed states.

Nucleotide Binding and NBD Movement. A number of studies have indicated a strong cooperativity between the two NBDs during the catalytic cycle (*64*) and that two functional NBDs are a prerequisite for normal rates of ATP hydrolysis and transporter function (*65*, *66*). These data suggest that core elements of one NBD interact or cooperate with those of the other. In a model of the ATP-bound histidine importer NBD dimer, the Signature motif of one NBD is positioned such that it completes the ATP-binding pocket of the other NBD (*13*). ATP is sandwiched between the Walker A motif of one NBD and the Signature motif of the other, and it is thought that this may represent a universal model of NBD dimerization; indeed, this arrangement was found in the structures of the Rad50cd NBDs (*20*) and the MJ0796 NBDs (*60*), and also suggested by photocleavage experiments and structures of MalK (*58*, *67*). Interestingly, superposition of the ATP-binding pockets of BtuCD and Rad50 (*17*) reveals that the Signature motif in BtuCD is slightly further away from the nucleotide-binding site relative to Rad50, and Locher and co-workers suggested that binding of ATP to BtuCD might confer a more Rad50-like conformation, with a "closing" of the NBD interface. In analyzing our current simulations, we aimed to address how the nucleotide-binding site changes in the ATP-bound simulations and what are the more global effects of any changes on the association of the NBDs?

In order to analyze the role of nucleotide-binding residues of the NBDs during the ATP-bound simulations, the H-bonding interactions of ATP with neighboring protein atoms were monitored, using LIGPLOT (*68*) and VMD (*49*), while monitoring intermotif distances as a function of time. In the initial structure, the ATP is hydrogen-bonded exclusively to residues in and around the Walker A motif of its most proximal NBD, with the Signature motif of the other NBD too distant to make hydrogen bonds. Over the first half of the BtuD-ATP simulation, a decrease in the distance between the Walker A-ATP hydrogen-bonding network and the Signature motif of the opposite NBD was observed (Figure 5). This movement was characterized by an initial motion of the base and sugar moieties of the ATP molecule toward the Signature motif, with the phosphates firmly bound to the Walker A motif. Interestingly, in the latter half of the BtuD-ATP simulation, the motion continues at one site, bringing the Signature motif of the opposite NBD close enough to complete the ATP-binding pocket, forming multiple hydrogen bonds with the phosphate and sugar moieties of ATP (Figure 5). We have compared the structure of this binding site to the structure of the homologous binding site in the Rad50 crystal structure, by calculating the RMSD of the conserved Walker A and Signature motif residues, as well as the α, β, and γ ATP phosphate atoms. At the start of the simulation (i.e., comparing crystal structures) there is an RMSD of 0.24 nm, which reduces to 0.18 nm after 15 ns, showing that the BtuD binding site adopts a conformation more similar to Rad50 than in the crystal structure. At the other ATP-binding site, there is no further closure of the binding site, and the binding pocket is consequently less tightly packed, although hydrogen bonds between the Signature motif and ATP are still seen. This ATP-driven association is in agreement with structural and biochemical studies of NBD dimers (*69*−*71*).

In contrast, the ATP-bound BtuCD simulation does not show any such change at either binding site, and after 15 ns, the Signature motif had not moved closer to the ATP molecule. In fact, the distance between the Signature motif and the Walker A motif actually increases slightly, implying a mild relaxation of the binding site (Figure 5). This is an interesting result in light of the effect of ATP in the BtuD simulation and appears to contradict the observation in a previous BtuCD simulation study that closure of one ATP-binding site is accompanied by opening of the opposite ATP-binding site (*31*). It may be that multiple extended simulations are needed to resolve this apparent difference.

Global motions of the NBDs (which are likely linked to the events at the ATP-binding site) have been analyzed via the distance between the centers-of-mass of each NBD over the simulations, thus providing an indication of their degree of association. For the BtuD simulations (Figure 6), we see

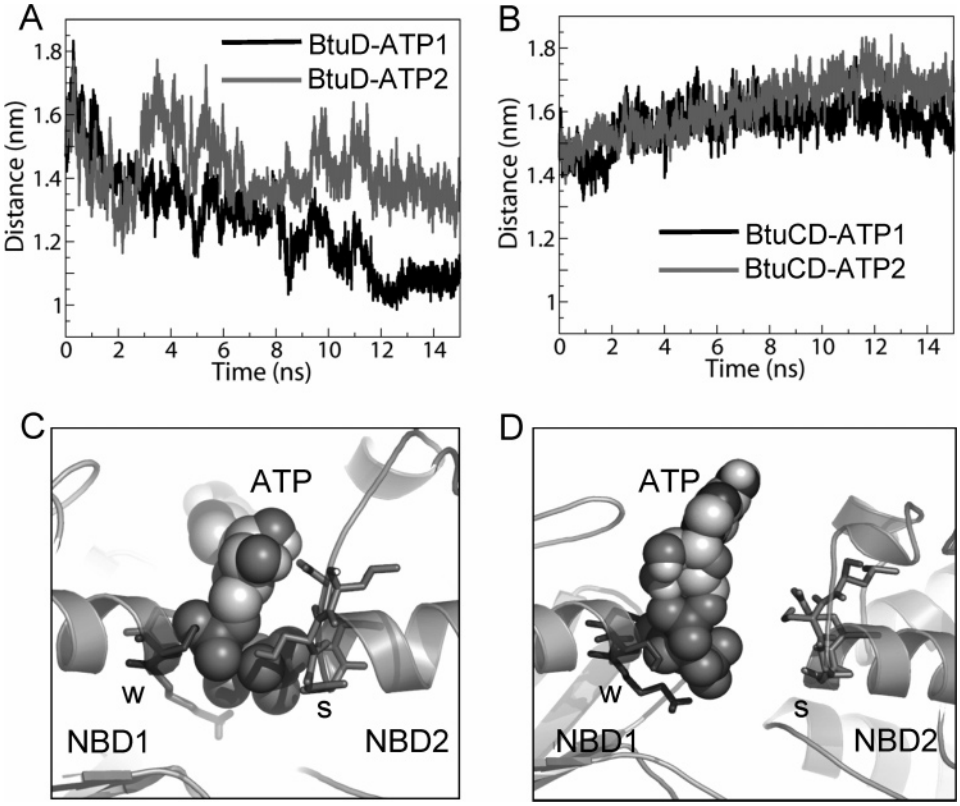

FIGURE 5: Distances between the centers of mass of the Walker A motif and the Signature motif in the (A) BtuD ATP and (B) BtuCD ATP simulations. Both nucleotide-binding sites of the dimers are analyzed. ATP1 is defined as the ATP molecule bound to the Walker A motif which occurs first in the BtuCD sequence (residues 685−687 in BtuCD and 37−39 in BtuD) and ATP2 as the ATP molecule bound to the second Walker A motif (residues 916−918 in BtuCD and 268−270 in BtuD). The Signature motif binding to ATP1 includes residues 1005−1009 in BtuCD and 357−361 in BtuD, and the Signature motif binding to ATP2 includes residues 774−778 in BtuCD and 126−130 in BtuD. C,D. Snapshots of ATP-binding site 1 at 15 ns from (A) BtuD and (B) BtuCD. Walker A residues are in dark gray (stick representation, labeled w); signature motif residues are colored in pale gray (stick representation, labeled s).

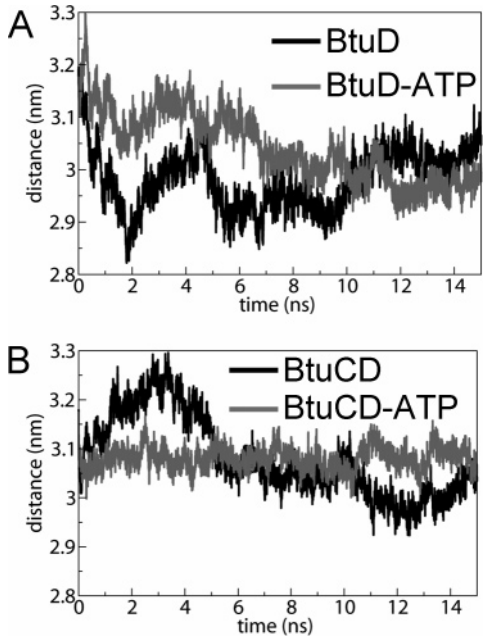

FIGURE 6: Distance between center-of-mass of NBDs as a function of time for (A) BtuD (black) and BtuD ATP (gray) and (B) BtuCD (black) and BtuCD ATP (gray).

that, in the absence of bound ATP, the inter-NBD distance fluctuates between opening/closing movements, whereas in the presence of bound ATP, the domains gradually move closer to each other, as was also suggested by the combined PCA and the "ATP-binding" results. In the BtuCD simulations (Figure 6), one may again see opening and closing motions of the NBDs in the absence of ATP. However, in the presence of ATP, the inter-NBD distance does not change significantly, which reflects the absence of any conformational change at the ATP-binding sites. Clearly, ATP has a different effect on the motion of the NBDs in the two systems.

Effects of BtuF. How might the lack of ATP-driven closure of the NBDs of the intact transporter be reconciled with existing biochemical data and transport models? Recent studies of a PgP mutant, in which the NBD dimer has been stabilized, have shown that the binding of solute to the transporter accelerates dimerization of the NBDs and "occlusion" of nucleotide within the binding site, relative to the solute-free state (*72*). Furthermore, this solute-driven increase in nucleotide binding could be shut down by mutation of two conserved glutamine residues which lie in the Q-loop and which are proposed to mediate communication between the drug and nucleotide-binding sites (*73*). Work on the bacterial maltose import complex $MalFGK_2$ has shown that on its own this transporter does not hydrolyze ATP, but addition of liganded maltose binding protein (MBP) stimulates hydrolytic activity of the NBDs (*74*). It is feasible that this stimulation is an allosteric effect which may bring the ATP-bound NBDs into closer proximity and thus render them catalytically active. It has also been suggested that, in the full transporter, ATP binds to the NBDs, with the TMDs

acting as a kind of "lock", preventing NBD dimerization until the arrival of the solute (*75*). However, in contrast to $MalFGK_2$, BtuCD seems to have a significant basal rate of ATP hydrolysis in the absence of BtuF, but one which is increased in the presence of BtuF (*76*). Together, these results imply that the NBDs of BtuCD, in the absence of the periplasmic binding protein (BtuF) and its B_{12} ligand, may either not be expected to close any further than in the crystal structure, or at least may not be expected to close on a time scale accessible to MD (*76*). We therefore extended our systems to include BtuF, to see if it could alter the dynamics of the intact transporter.

BtuF is a periplasmic binding protein, with a vitamin B_{12} binding site in a cleft between two lobes (domains). The availability of high-resolution crystal structures of the vitamin B_{12} bound and ligand-free (i.e., apo) conformations of BtuF (*19*, *35*) provides an opportunity to study the complete vitamin B_{12} import complex via MD simulations. Recent studies on the maltose import complex suggest that NBD closure in the presence of ATP is coupled to PBP opening and consequent release of substrate into the periplasmic entrance to the transporter (*77*). In our simulations of BtuCDF, we wished to examine whether the presence of BtuF had any effect, on a multi-nanosecond time scale, on the association of the NBDs.

As a first step, the structure of apo BtuF (*19*) was simulated in water for 20 ns. PCA of this trajectory reveals that the dominant movements of the protein are symmetrical breathing motions of the two lobes moving relative to the other. This is suggestive of a mechanism of conformational change allowing binding/release of vitamin B_{12} from the interlobe cleft. Although we note that such a conformational change has not been observed with X-ray crystallography, in that the bound and apo states of BtuF have similar crystal structures (*19*), a recent simulation study of BtuF (*34*) suggests that it may be more flexible than anticipated. The breathing motions observed suggested that perhaps the lobes of BtuF push on the periplasmic ends of the TMDs in order to force open the periplasmic entrance of the translocation pathway for the delivery of vitamin B_{12}. To examine whether these motions were seen in the full BtuCDF complex, BtuF was docked onto BtuCD (Figure 7A), and simulations in the presence/absence of bound ATP were performed. PCA of the resultant trajectories of the complete BtuCDF complex revealed changes which occurred upon docking of BtuF. The most notable motion is seen in the principal component of the nucleotide-free BtuCDF simulation, where the outward movement of the lobes of BtuF is coupled to the closing motion of the NBDs (Figure 7), mediated through a similar "shearing" motion of the TMDs to that observed in the principal component of the BtuCD simulation. As anticipated, the lobes of BtuF move in tandem with the proximal periplasmic ends of the TMDs. This motion is of interest in light of the proposal that the maltose PBP stabilizes the transition state for ATP hydrolysis while concurrently losing its high affinity for maltose (*77*). This motion could satisfy both effects: NBD closure would bring together the catalytic residues of both NBD subunits for hydrolysis and PBP opening would prize apart the B_{12}-binding residues around the cleft and facilitate the movement of B_{12} from the PBP to the TMDs.

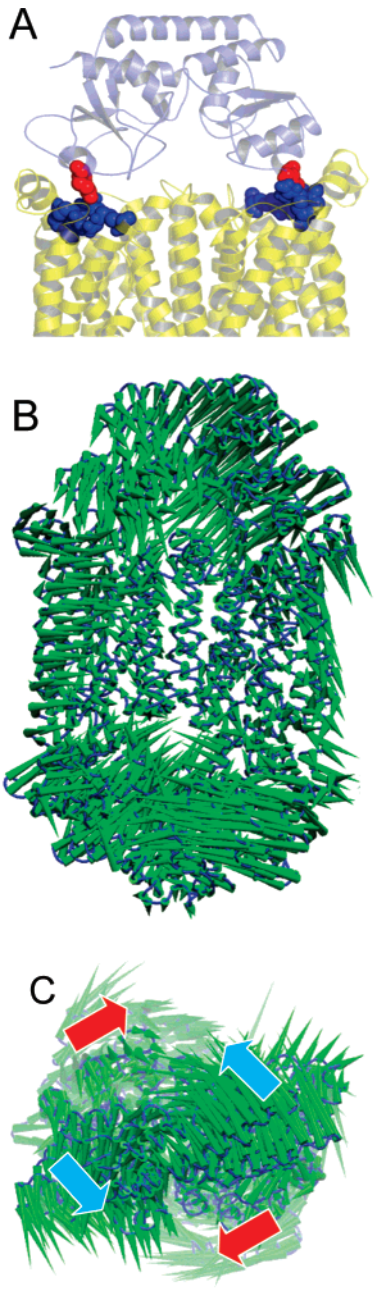

FIGURE 7: A. The model of the BtuCDF complex, showing the "front view" of the BtuC-BtuF interface. The conserved Glu and Arg residues used in the docking of BtuF are shown in red and blue, respectively. BtuF and BtuC subunits are shown in dark blue and yellow, respectively (cartoon representation). The NBDs are omitted for clarity. B,C. Principal components analysis of the BtuCDF simulation. Porcupine plots of (B) front view and (C) periplasmic view. Arrows indicate opposing motion of BtuF lobes (blue) and NBDs (red).

Does NBD association differ in the presence and absence of BtuF? We repeated the inter-NBD distance calculations on the BtuCDF complex and found that in both the presence and absence of ATP simulations there was a closure of the NBDs (Figure 8). In the BtuCDF simulation (i.e., in the absence of ATP), the behavior of the inter-NBD distance over time was similar to that of the BtuCD simulation. However, when we compare the BtuCDF-ATP distances to those of BtuCD-ATP, a significant decrease is seen in the presence of BtuF, suggesting an association of the NBDs which we did not see in the absence of the periplasmic

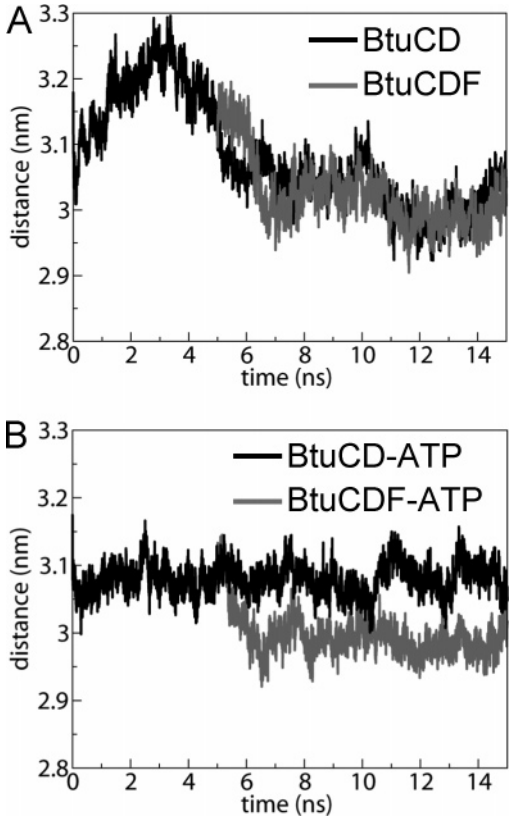

FIGURE 8: Distance between center-of-mass of NBDs as a function of time for (A) BtuCD vs BtuCDF and (B) BtuCD ATP vs BtuCDF ATP.

binding protein. This closer association is retained for the remainder of the simulation, and the final inter-NBD distance is comparable to the final distance seen in the ATP-bound NBD dimer (Figure 6). When we look at the events at the ATP-binding sites, by measuring the distance between the Walker A motif and the Signature motif of the opposing NBD and comparing to the BtuF-free system (results not shown), we see a sharp closure of one binding site, with no apparent change at the other site. This striking asymmetry, which is not seen in our NBD dimer simulation, or indeed any of the crystal structures of nucleotide-bound NBD dimers, therefore appears to be imposed by the presence of the TMDs. Nucleotide-binding stoichiometries have been measured for both the eukaryotic PgP (*72*) and the prokaryotic BmrA (*78*), in which mutations have been made which dramatically reduce hydrolysis and therefore promote a nucleotide-bound state. These studies have revealed a stoichiometry of 1 mol nucleotide per mole of transporter and thus lead to the suggestion that the NBDs of full transporters may transiently bind ATP more tightly at one site after ATP has initially bound to both sites (*72*). We believe that the binding seen in our simulation of the ATP-bound full complex correlates with the step of the alternating sites model (*56*) in which ATP preferentially binds to one NBD, preventing the other from doing so. This asymmetrical binding of ATP may have implications for the observations that hydrolysis is also asymmetrical, for example, as seen in experiments on PgP (*79*) and the prokaryotic LmrA (*8*) and $MalFGK_2$ (*80*). Interestingly, the recent crystal structure of nucleotide-bound MsbA reveals the presence of ADP-vanadate at only a single site, providing structural evidence of sequential binding/hydrolysis, even in a "symmetrical" homodimer (*16*).

It is significant that BtuF is able to promote NBD association even in the absence of the B_{12} ligand in our simulations. Recent experimental studies on the BtuCDF complex have shown an apparent insensitivity of the BtuF-driven stimulation of BtuCD ATP hydrolysis to the presence or absence of vitamin B_{12} (*76*).

CONCLUSIONS

Despite the brevity of the simulations relative to the turnover time of ABC transporters, a number of aspects of the conformational dynamics observed in our simulations have possible mechanistic implications.

First, it appears that binding of ATP drives closure of the NBDs in BtuD but not in BtuCD. This contrasts with previous simulations performed on BtuCD (*31*) whereby binding of Mg-ATP to the NBDs was able to elicit a closure of the gap between the ATP-binding cassettes. In our studies, the distance between the center-of-mass of each NBD does not change appreciably with ATP bound. Also, in the ATP-free state, the previous study observed that the NBDs of BtuCD drifted apart over 15 ns, whereas our simulations show that the NBDs fluctuate between "open" and "closed" states (i.e., states that are either more open or more closed than the crystal structure). In the previous study (*31*), it was also observed that closure of one ATP-binding site is coupled to the opening of the opposite site. Again, such activity at the ATP-binding sites is not observed in BtuCD in our studies—both sites appear to open slightly, in a concerted fashion. These differences between the two studies may reflect differences either in the way in which Mg-ATP was modeled into the BtuCD structure and/or in the lipids (DMPC vs POPE) used in the bilayer. However, it is difficult to be certain of this without detailed comparisons of the two sets of simulations (*81*).

In our simulations of BtuCD, it seems that ATP effectively "locks" the NBDs (constraining their flexibility), such that their closure can only occur upon binding of BtuF to the complex. This is consistent with observations that solute binding is required to trigger ATP-binding/hydrolysis (*72*, *74*). The closure of the NBDs in BtuCDF is asymmetrical, which is consistent with of "alternating hydrolysis" models (*8*, *56*) and stoichiometric calculations (*72*, *82*). Interestingly, our observations of events at the ATP-binding sites for the BtuCDF complex are reconcilable with the asymmetrical behavior seen in the previous, somewhat less extensive, simulation studies of BtuCD (*31*). Upon introduction of BtuF, and concomitant with NBD association, one ATP-binding site shows a dramatic closure, while the opposite site remains unchanged (relative to the same site in BtuCD; results not shown). However, it should be noted that there is also evidence favoring the idea of symmetrical binding of ATP to the two NBDs (as observed in our NBD-only simulations). Structural evidence has previously relied on symmetrical nucleotide-bound NBD dimer configurations (such as Rad50 and MalK), though their relevance to the active complex has been questioned, as they both lack the TMDs and are hydrolytically inactive. More recently, the SAV1866 structure has revealed the symmetrical binding of ADP to the NBDs of an intact transporter (*18*). Further studies will be required to elucidate the nucleotide-binding mechanism.

The principal components analysis of the simulated motions of BtuCD has been especially informative. The motions observed are comparable to those suggested in Davidson's transport model (*21*) and experimental studies on MsbA (*54*). It is also tempting to speculate that a similar motion exists for exporters, with the roles of ATP binding and hydrolysis reversed, as has been suggested in ref 18, i.e., ATP binding providing for escape of the solute into the extracellular medium and ATP hydrolysis "resetting" the transporter to an inward-facing conformation. PCA also seems to confirm that ATP "drives" NBD closure in BtuD, while the apo-state (i.e., no nucleotide bound) of BtuD randomly switches between an open and closed state.

From a methodological perspective, there are a number of areas which require consideration. As in nearly all current MD simulations of membrane proteins, it would desirable to access longer time scales in order to provide better conformational sampling. In particular, it is likely that larger conformational changes may be observed on longer time scales. Simulations on simpler systems (e.g., periplasmic binding proteins (*83*)) suggest that multiple extended simulations on a number of related ABC proteins may provide a route to improved sampling of conformation changes. Another route may be via multiscale simulations (*84*), possibly using elastic network models (*85*) to improve sampling of conformational changes.

From a biophysical perspective, a number of refinements are possible. The current simulations are in a simple PC bilayer—the possible effects of a more complex (and realistic) bilayer environment on ABC dynamics merits attention, given recent results in ion channel (*86*) and receptor (*87*) simulations. It would also be of interest to explore further the mechanism of hydrolysis of ATP by the NBDs, possibly via QM/MM methods (*88*), and to explore the effects of vitamin B12 binding to BtuF.

REFERENCES

1. Abele, R., and Tampe, R. (1999) Function of the transport complex TAP in cellular immune recognition, *Biochim. Biophys. Acta 1461*, 405−419.
2. Akabas, M. H. (2000) Cystic fibrosis transmembrane conductance regulator. Structure and function of an epithelial chloride channel, *J. Biol. Chem. 275*, 3729−3732.
3. Ehrmann, M., Ehrle, R., Hofmann, E., Boos, W., and Schlosser, A. (1998) The ABC maltose transporter, *Mol. Microbiol. 29*, 685−694.
4. Doerrler, W. T., and Raetz, C. R. (2002) ATPase activity of the MsbA lipid flippase of *Escherichia coli*, *J. Biol. Chem. 277*, 36697−36705.
5. Rosenberg, M. F., Callaghan, R., Ford, R. C., and Higgins, C. F. (1997) Structure of the multidrug resistance P-glycoprotein to 2.5 nm resolution determined by electron microscopy and image analysis, *J. Biol. Chem. 272*, 10685−10694.
6. Liu, C. E., Liu, P. Q., and Ames, G. F. (1997) Characterization of the adenosine triphosphatase activity of the periplasmic histidine permease, a traffic ATPase (ABC transporter), *J. Biol. Chem. 272*, 21883−91.
7. Holland, I. B. C., P. C. S., Kuchler, K., and Higgins, C. F. (2003) Academic Press, London.
8. van Veen, H. W., Margolles, A., Muller, M., Higgins, C. F., and Konings, W. N. (2000) The homodimeric ATP-binding cassette transporter LmrA mediates multidrug transport by an alternating two-site (two-cylinder engine) mechanism, *EMBO J. 19*, 2503−14.
9. Gottesman, M. M., Fojo, T., and Bates, S. E. (2002) Multidrug resistance in cancer: role of ATP-dependent transporters, *Nat. Rev. Cancer 2*, 48−58.
10. Chen, J. M., Cutler, C., Jacques, C., Boeuf, G., Denamur, E., Lecointre, G., Mercier, B., Cramb, G., and Ferec, C. (2001) A combined analysis of the cystic fibrosis transmembrane conductance regulator: implications for structure and disease models, *Mol. Biol. Evol. 18*, 1771−88.
11. Higgins, C. F. (2001) ABC Transporters: physiology, structure and mechanism - an overview, *Res. Microbiol. 152*, 205−210.
12. Holland, I. B., and Blight, M. A. (1999) ABC-ATPases, adaptable energy generators fuelling transmembrane movement of a variety of molecules organisms from bacteria to humans, *J. Mol. Biol. 293*, 381−399.
13. Jones, P. M., and George, A. M. (1999) Subunit interactions in ABC transporters: towards a functional architecture, *FEMS Microbiol. Lett. 179*, 187−202.
14. Chang, G., and Roth, C. B. (2001) Structure of MsbA from *E. coli*: a homolog of the multidrug resistance ATP binding cassette (ABC) transporters, *Science 293*, 1793−1800.
15. Chang, G. (2003) Structure of MsbA from *Vibrio cholera*: a multidrug resistance ABC transporter homolog in a closed conformation, *J. Mol. Biol. 330*, 419−430.
16. Reyes, C. L., and Chang, G. (2005) Structure of the ABC transporter MsbA in complex with ADP.vanadate and lipopolysaccharide, *Science 308*, 1028−1031.
17. Locher, K. P., Lee, A. T., and Rees, D. C. (2002) The *E. coli* BtuCD structure: a framework for ABC transporter architecture and mechanism, *Science 296*, 1091−1098.
18. Dawson, R. J., and Locher, K. P. (2006) Structure of a bacterial multidrug ABC transporter, *Nature (London) 443*, 180−185.
19. Karpowich, N. K., Huang, H. H., Smith, P. C., and Hunt, J. F. (2003) Crystal structures of the BtuF periplasmic-binding protein for vitamin B12 suggest a functionally important reduction in protein mobility upon ligand binding, *J. Biol. Chem. 278*, 8429−8434.
20. Hopfner, K. P., Karcher, A., Shin, D. S., Craig, L., Arthur, L. M., Carney, J. P., and Tainer, J. A. (2000) Structural biology of Rad50 ATPase: ATP-driven conformational control in DNA double-strand break repair and the ABC-ATPase superfamily, *Cell 101*, 789−800.
21. Davidson, A. L., and Chen, J. (2004) ATP-binding cassette transporters in bacteria, *Annu. Rev. Biochem. 73*, 241−268.
22. Reyes, C. L., Ward, A., Yu, J., and Chang, G. (2006) The structures of MsbA: Insight into ABC transporter-mediated multidrug efflux, *FEBS Lett. 580*, 1042−1048.
23. Karplus, M. J., and McCammon, J. A. (2002) Molecular dynamics simulations of biomolecules, *Nat. Struct. Biol. 9*, 646−652.
24. Adcock, S. A., and McCammon, J. A. (2006) Molecular dynamics: survey of methods for simulating the activity of proteins, *Chem. Rev. 106*, 1589−1615.
25. Ash, W. L., Zlomislic, M. R., Oloo, E. O., and Tieleman, D. P. (2004) Computer simulations of membrane proteins, *Biochim. Biophys. Acta 1666*, 158−189.
26. Roux, B., and Schulten, K. (2004) Computational studies of membrane channels, *Structure 12*, 1343−1351.
27. Campbell, J. D., and Sansom, M. S. P. (2005) Nucleotide binding to the homodimeric MJ0796 protein: a computational study of a prokaryotic ABC transporter NBD dimer, *FEBS Lett. 579*, 4193−4199.
28. Jones, P. M., and George, A. M. (2002) Mechanism of ABC transporters: A molecular dynamics simulation of a well characterized nucleotide-binding subunit, *Proc. Nat. Acad. Sci. U.S.A. 99*, 12639−12644.
29. Campbell, J. D., Deol, S. S., Ashcroft, F. M., Kerr, I. D., and Sansom, M. S. P. (2004) Nucleotide dependent conformational changes in HisP: molecular dynamics simulations of an ABC transporter nucleotide binding domain, *Biophys. J. 87*, 3703−3715.
30. Campbell, J. D., Biggin, P. C., Baaden, M., and Sansom, M. S. P. (2003) Extending the structure of an ABC transporter to atomic resolution: modelling and simulation studies of MsbA, *Biochemistry 42*, 3666−3673.
31. Oloo, E. O., and Tieleman, D. P. (2004) Conformational transitions induced by the binding of MgATP to the vitamin B12 ATP-binding cassette (ABC) transporter BtuCD, *J. Biol. Chem. 279*, 45013−9.
32. Tanizaki, S., and Feig, M. (2006) Molecular dynamics simulations of large integral membrane proteins with an implicit membrane model, *J. Phys. Chem. B 110*, 548−556.

33. Nikaido, K., Liu, P. Q., and Ames, G. F. (1997) Purification and characterization of HisP, the ATP-binding subunit of a traffic ATPase (ABC transporter), the histidine permease of *Salmonella typhimurium*. Solubility, dimerization, and ATPase activity, *J. Biol. Chem. 272*, 27745−27752.
34. Kandt, C., Xu, Z., and Tieleman, D. P. (2006) Opening and closing motions in the periplasmic vitamin B_{12} binding protein BtuF, *Biochemistry 45*, 13284−13292.
35. Borths, E. L., Locher, K. P., Lee, A. T., and Rees, D. C. (2002) The structure of *Escherichia coli* BtuF and binding to its cognate ATP binding cassette transporter, *Proc. Natl. Acad. Sci. U.S.A. 99*, 16642−16647.
36. Berendsen, H. J. C., Postma, J. P. M., van Gunsteren, W. F., DiNola, A., and Haak, J. R. (1984) Molecular dynamics with coupling to an external bath, *J. Chem. Phys. 81*, 3684−3690.
37. Nose, S. (1984) A molecular dynamics method for simulations in the canonical ensemble, *Mol. Phys. 52*, 255−268.
38. Hoover, W. G. (1985) Canonical dynamics: equilibrium phase-space distributions, *Phys. Rev. A31*, 1695−1697.
39. Parrinello, M., and Rahman, A. (1981) Polymorphic transitions in single-crystals - a new molecular-dynamics method, *J. Appl. Phys. 52*, 7182−7190.
40. Darden, T., York, D., and Pedersen, L. (1993) Particle mesh Ewald - an N.log(N) method for Ewald sums in large systems, *J. Chem. Phys. 98*, 10089−10092.
41. Hermans, J., Berendsen, H. J. C., van Gunsteren, W. F., and Postma, J. P. M. (1984) A consistent empirical potential for water-protein interactions, *Biopolymers 23*, 1513−1518.
42. Hess, B., Bekker, H., Berendsen, H. J. C., and Fraaije, J. G. E. M. (1997) LINCS: A linear constraint solver for molecular simulations, *J. Comput. Chem. 18*, 1463−1472.
43. Berendsen, H. J. C., van der Spoel, D., and van Drunen, R. (1995) GROMACS: A message-passing parallel molecular dynamics implementation, *Comput. Phys. Comm. 95*, 43−56.
44. Lindahl, E., Hess, B., and van der Spoel, D. (2001) GROMACS 3.0: a package for molecular simulation and trajectory analysis, *J. Mol. Model. 7*, 306−317.
45. van der Spoel, D., Lindahl, E., Hess, B., Groenhof, G., Mark, A. E., and Berendsen, H. J. (2005) *GROMACS: fast, flexible, and free*, Vol. 26.
46. Scott, W. R. P., Hunenberger, P. H., Tironi, I. G., Mark, A. E., Billeter, S. R., Fennen, J., Torda, A. E., Huber, T., Kruger, P., and van Gunsteren, W. F. (1999) The GROMOS biomolecular simulation program package, *J. Phys. Chem. A 103*, 3596−3607.
47. Berger, O., Edholm, O., and Jahnig, F. (1997) Molecular dynamics simulations of a fluid bilayer of dipalmitoylphosphatidycholine at full hydration, constant pressure and constant temperature, *Biophys. J. 72*, 2002−2013.
48. Smart, O. S., Neduvelil, J. G., Wang, X., Wallace, B. A., and Sansom, M. S. P. (1996) Hole: A program for the analysis of the pore dimensions of ion channel structural models, *J. Mol. Graphics 14*, 354−360.
49. Humphrey, W., Dalke, A., and Schulten, K. (1996) VMD - Visual Molecular Dynamics, *J. Mol. Graphics 14*, 33−38.
50. Arinaminpathy, Y., Sansom, M. S. P., and Biggin, P. C. (2002) Molecular dynamics simulations of the ligand binding domain of the ionotropic glutamate receptor, GluR2, *Biophys. J. 82*, 676−683.
51. Amadei, A., Linssen, A. B. M., and Berendsen, H. J. C. (1993) Essential dynamics of proteins, *Proteins: Struct., Funct., Genet. 17*, 412−425.
52. Ambudkar, S. V., Cardarelli, C. O., Pashinskyi, I., and Stein, W. D. (1997) Relation between the turnover number for vinblastine transport and for vinblastine-stimulated ATP hydrolysis by human P-glycoprotein, *J. Biol. Chem. 272*, 21160−21166.
53. Haider, S., Grottesi, A., Hall, B. A., Ashcroft, F. M., and Sansom, M. S. P. (2005) Conformational dynamics of the ligand-binding domain of inward rectifier K channels as revealed by MD simulations: towards an understanding of Kir channel gating, *Biophys. J. 88*, 3310−3320.
54. Grottesi, A., Domene, C., and Sansom, M. S. P. (2005) Conformational dynamics of M2 helices in KirBac channels: helix flexibility in relation to gating via molecular dynamics simulations, *Biochemistry 44*, 14586−14594.
55. Dong, J., Yang, G., and McHaourab, H. S. (2005) Structural basis of energy transduction in the transport cycle of MsbA, *Science 308*, 1023−1028.
56. Senior, A. E., al-Shawi, M. K., and Urbatsch, I. L. (1995) The catalytic cycle of P-glycoprotein, *FEBS Lett. 377*, 285−9.
57. Higgins, C. F., and Linton, K. J. (2004) The ATP switch model for ABC transporters, *Nat. Struct. Mol. Biol. 11*, 918−926.
58. Chen, J., Lu, G., Lin, J., Davidson, A. L., and Quiocho, F. A. (2003) A tweezers-like motion of the ATP-binding cassette dimer in an ABC transport cycle, *Mol. Cell 12*, 651−661.
59. Loo, T. W., Bartlett, M. C., and Clarke, D. M. (2002) The "LSGGQ" motif in each nucleotide-binding domain of human p-glycoprotein is adjacent to the opposing Walker A sequence, *J. Biol. Chem. 277*, 41303−41306.
60. Smith, P. C., Karpowich, N., Millen, L., Moody, J. E., Rosen, J., Thomas, P. J., and Hunt, J. F. (2002) ATP binding to the motor domain from an ABC transporter drives formation of a nucleotide sandwich dimer, *Mol. Cell 10*, 139−149.
61. Moody, J. E., Millen, L., Binns, D., Hunt, J. F., and Thomas, P. J. (2002) Cooperative, ATP-dependent association of the nucleotide binding cassettes during the catalytic cycle of ATP-binding cassette transporters, *J. Biol. Chem. 277*, 21111−21114.
62. Verdon, G., Albers, S. V., Dijkstra, B. W., Driessen, A. J., and Thunnissen, A. M. (2003) Crystal structures of the ATPase subunit of the glucose ABC transporter from *Sulfolobus solfataricus*: nucleotide-free and nucleotide-bound conformations, *J. Mol. Biol. 330*, 343−358.
63. van Aalten, D. M., Findlay, J. B., Amadei, A., and Berendsen, H. J. (1995) Essential dynamics of the cellular retinol-binding protein−evidence for ligand-induced conformational changes, *Protein Eng. 8*, 1129−1135.
64. Davidson, A. L., Laghaeian, S. S., and Mannering, D. E. (1996) The maltose transport system of *Escherichia coli* displays positive cooperativity in ATP hydrolysis, *J. Biol. Chem. 271*, 4858−4863.
65. Berkower, C., and Michaelis, S. (1991) Mutational analysis of the yeast a-factor transporter STE6, a member of the ATP binding cassette (ABC) protein superfamily, *EMBO J. 10*, 3777−3785.
66. Davidson, A. L., and Sharma, S. (1997) Mutation of a single MalK subunit severely impairs maltose transport activity in *Escherichia coli*, *J. Bacteriol. 179*, 5458−5464.
67. Fetsch, E. E., and Davidson, A. L. (2002) Vanadate-catalyzed photocleavage of the signature motif of an ATP-binding cassette (ABC) transporter, *Proc. Natl. Acad. Sci. U.S.A. 99*, 9685−9690.
68. Wallace, A. C., Laskowski, R. A., and Thornton, J. M. (1995) LIGPLOT: a program to generate schematic diagrams of protein-ligand interactions, *Protein Eng. 8*, 127−134.
69. Janas, E., Hofacker, M., Chen, M., Gompf, S., van der Does, C., and Tampe, R. (2003) The ATP hydrolysis cycle of the nucleotide-binding domain of the mitochondrial ATP-binding cassette transporter Mdl1p, *J. Biol. Chem. 278*, 26862−26869.
70. Verdon, G., Albers, S. V., van Oosterwijk, N., Dijkstra, B. W., Driessen, A. J., and Thunnissen, A. M. (2003) Formation of the productive ATP-Mg2+-bound dimer of GlcV, an ABC-ATPase from *Sulfolobus solfataricus*, *J. Mol. Biol. 334*, 255−267.
71. Zaitseva, J., Jenewein, S., Jumpertz, T., Holland, I. B., and Schmitt, L. (2005) H662 is the linchpin of ATP hydrolysis in the nucleotide-binding domain of the ABC transporter HlyB, *EMBO J. 24*, 1901−1910.
72. Tombline, G., Muharemagic, A., White, L. B., and Senior, A. E. (2005) Involvement of the "occluded nucleotide conformation" of P-glycoprotein in the catalytic pathway, *Biochemistry 44*, 12879−12886.
73. Urbatsch, I. L., Gimi, K., Wilke-Mounts, S., and Senior, A. E. (2000) Investigation of the role of glutamine-471 and glutamine-1114 in the two catalytic sites of P-glycoprotein, *Biochemistry 39*, 11921−11927.
74. Davidson, A. L., Shuman, H. A., and Nikaido, H. (1992) Mechanism of maltose transport in *Escherichia coli*: transmembrane signaling by periplasmic binding proteins, *Proc. Natl. Acad. Sci. U.S.A. 89*, 2360−2364.
75. Hanekop, N., Zaitseva, J., Jenewein, S., Holland, I. B., and Schmitt, L. (2006) Molecular insights into the mechanism of ATP-hydrolysis by the NBD of the ABC-transporter HlyB, *FEBS Lett. 580*, 1036−1041.
76. Borths, E. L., Poolman, B., Hvorup, R. N., Locher, K. P., and Rees, D. C. (2005) In vitro functional characterization of BtuCD-F, the *Escherichia coli* ABC transporter for vitamin B12 uptake, *Biochemistry 44*, 16301−16309.
77. Austermuhle, M. I., Hall, J. A., Klug, C. S., and Davidson, A. L. (2004) Maltose-binding protein is open in the catalytic transition state for ATP hydrolysis during maltose transport, *J. Biol. Chem. 279*, 28243−28250.
78. Orelle, C., Dalmas, O., Gros, P., Di Pietro, A., and Jault, J. M. (2003) The conserved glutamate residue adjacent to the Walker-B

motif is the catalytic base for ATP hydrolysis in the ATP-binding cassette transporter BmrA, *J. Biol. Chem. 278*, 47002−8.
79. Senior, A. E., and Gadsby, D. C. (1997) ATP hydrolysis cycles and mechanism in P-glycoprotein and CFTR, *Semin. Cancer Biol. 8*, 143−50.
80. Chen, J., Sharma, S., Quiocho, F. A., and Davidson, A. L. (2001) Trapping the transition state of an ATP-binding cassette transporter: evidence for a concerted mechanism of maltose transport, *Proc. Natl. Acad. Sci. U.S.A. 98*, 1525−1530.
81. Tai, K., Murdock, S., Wu, B., Ng, M. H., Johnston, S., Fangohr, H., Cox, S. J., Jeffreys, P., Essex, J. W., and Sansom, M. S. P. (2004) BioSimGrid: towards a worldwide repository for biomolecular simulations, *Org. Biomol. Chem. 2, 3219−3221*.
82. Orelle, C., Dalmas, O., Gros, P., Di Pietro, A., and Jault, J. M. (2003) The conserved glutamate residue adjacent to the Walker-B motif is the catalytic base for ATP hydrolysis in the ATP-binding cassette transporter BmrA, *J. Biol. Chem. 278*, 47002−8.
83. Pang, A., Arinaminpathy, Y., Sansom, M. S. P., and Biggin, P. C. (2005) Comparative molecular dynamics - similar folds and similar motions? *Proteins: Struct., Funct., Bioinf. 61*, 809−822.
84. Praprotnik, M., Delle Site, L., and Kremer, K. (2005) Adaptive resolution molecular-dynamics simulation: Changing the degrees of freedom on the fly, *J. Chem. Phys. 123*, 224106.
85. Atilgan, A. R., Durell, S. R., Jernigan, R. L., Demirel, M. C., Keskin, O., and Bahar, I. (2001) Anisotropy of fluctuation dynamics of proteins with an elastic network model, *Biophys. J. 80*, 505−515.
86. Deol, S. S., Domene, C., Bond, P. J., and Sansom, M. S. P. (2006) Anionic phospholipids interactions with the potassium channel KcsA: simulation studies, *Biophys. J. 90*, 822−830.
87. Feller, S. E., Gawrisch, K., and Woolf, T. B. (2003) Rhodopsin exhibits a preference for solvation by polyunsaturated docosohexaenoic acid, *J. Am. Chem. Soc. 125*, 4434−4435.
88. Ridder, L., and Mulholland, A. J. (2003) Modeling biotransformation reactions by combined quantum mechanical/molecular mechanical approaches: from structure to activity, *Curr. Top. Med. Chem. 3*, 1241−1256.

BI0622571